

A numerical method for computing time-periodic solutions in dissipative wave systems

Jianke Yang

*Department of Mathematics and Statistics,
University of Vermont, Burlington, VT 05401, USA
email: jyang@math.uvm.edu*

A numerical method is proposed for computing time-periodic and relative time-periodic solutions in dissipative wave systems. In such solutions, the temporal period, and possibly other additional internal parameters such as the propagation constant, are unknown priori and need to be determined along with the solution itself. The main idea of the method is to first express those unknown parameters in terms of the solution through quasi-Rayleigh quotients, so that the resulting integro-differential equation is for the time-periodic solution only. Then this equation is computed in the combined spatiotemporal domain as a boundary value problem by Newton-conjugate-gradient iterations. The proposed method applies to both stable and unstable time-periodic solutions; its numerical accuracy is spectral; it is fast-converging; and its coding is short and simple. As numerical examples, this method is applied to the Kuramoto-Sivashinsky equation and the cubic-quintic Ginzburg-Landau equation, whose time-periodic or relative time-periodic solutions with spatially-periodic or spatially-localized profiles are computed. This method also applies to systems of ordinary differential equations, as is illustrated by its simple computation of periodic orbits in the Lorenz equations. MATLAB codes for all numerical examples are provided in appendices to illustrate the simple implementation of the proposed method.

I. INTRODUCTION

In studies of nonlinear waves in physical systems, coherent structures play a prominent role. The simplest coherent structures are stationary or traveling waves, which do not change their shape upon propagation. A familiar example is solitary waves in various physical wave equations (such as the Korteweg-de Vries equation). Another important class of coherent structures is time-periodic solutions, which change their shape periodically upon propagation. A familiar example is breathers in the sine-Gordon equation. Coherent structures are important for nonlinear wave equations for obvious reasons. If these structures are stable, they would serve as attractors and dictate solution dynamics. Even if they are unstable, they could still exert strong influence on the dynamical outcome (such as contributing to chaotic behaviors). Thus determination of coherent structures is a fundamental step toward the understanding of nonlinear wave systems. This determination is often numerical due to lack of analytical expressions.

If the wave system is conservative (i.e., without gain or loss), these coherent structures generally exist as continuous families, parameterized by their energy (or a related parameter such as wave height). Solitary waves in the Korteweg-de Vries equation are such examples, where the height of the wave is a free parameter. If the wave system is dissipative, however, these coherent structures generally exist as isolated objects, at discrete energy levels, due to the requirement that the gain and loss of the energy must balance each other exactly. Solitary waves in the complex Ginzburg-Landau equation are such examples, where the height of the solitary wave is fixed [1].

Numerical computations of stationary and traveling waves in nonlinear systems has a long history, and a large number of effective numerical methods have been developed (see [2] and the references therein). Most of these methods were designed for conservative systems, but some methods for dissipative systems are also available [1, 3].

In this article, we consider computations of time-periodic solutions in dissipative wave systems. This computation is more challenging than in conservative systems, because the solution's temporal period, as well as possibly other additional parameters, is discrete, but such parameters are not known priori and have to be computed together with the solution itself. So far, several numerical methods have been used for these computations. If the solution is stable, then it can be obtained as the long-time limit of an initial value problem by evolution simulation. This evolution method is often slow. More seriously, it cannot access unstable solutions, which are needed in many situations (such as a bifurcation study or estimation of fractal dimensions of a chaotic attractor [4]). A second method is the damped Newton's method, which was used on the Kuramoto-Sivashinsky equation [5]. In this method, the Kuramoto-Sivashinsky equation was discretized in the spatiotemporal domain by finite differences, and the resulting system of algebraic equations was solved by damped Newton iterations. A third method is based on error minimization and infinitesimal damped Newton iterations [6]. This method was developed for ordinary differential equations (ODEs), and then applied to the Kuramoto-Sivashinsky equation after it was converted to a system of ODEs through Fourier-

series expansion. A fourth method was used for computing relative time-periodic solutions of the complex Ginzburg-Landau equation under periodic boundary conditions [7]. In this method, the solution was expanded into space-time Fourier series, so that the Ginzburg-Landau equation was converted into a system of nonlinear algebraic equations, which was then solved by a nonlinear least squares solver from the MINPACK software package. One more method was used for computing time-periodic and space-localized solutions in the damped-driven nonlinear Schrödinger equation [8]. In this method, the wave equation was discretized in the spatiotemporal domain by finite differences into a set of nonlinear algebraic equations, which was then solved by Newton iterations.

Computations of time-periodic solutions in partial differential equations (PDEs) is closely related to computations of periodic orbits in systems of ODEs. For systems of ODEs, quite a few numerical methods are available. Examples include the multipoint shooting method [9], the finite-difference discretization method, the collocation method [10, 11], the multipoint-shooting with automatic differentiation method [12], and so on (the software package AUTO uses the B-spline collocation method [13]). In principle, all these ODE-based methods can be adapted to PDEs if the PDEs are first converted into a system of ODEs (by finite difference or spatial-mode expansion). However, the extra cost of PDE-to-ODE conversion and the inevitable large size of the resulting ODE system make such methods not ideal for PDE applications.

In this article, we develop a new numerical method for computing time-periodic and relative time-periodic solutions in dissipative wave equations. This work is motivated by several reasons. First, our view is that the best way to compute such solutions in PDEs is to do so in the PDE framework, rather than converting PDEs to large systems of ODEs or algebraic equations. The advantage of the PDE framework is that the structure of the PDE is retained, and important quantities such as the linearization operator of the PDE can be calculated analytically. Second, almost all numerical methods for time-periodic solutions in PDEs involve solving large systems of linear equations. Since conjugate-gradient methods are widely recognized as probably the fastest numerical method for solving linear algebraic and operator equations [14], we are motivated to incorporate conjugate-gradient methods into our algorithm. Thirdly, a good numerical algorithm should also be simple to implement. Since none of the previous numerical schemes provided sample codes for the readers to peruse, we are motivated to provide a set of simple sample codes, so that the readers can directly use them, or modify them for their own problems. Building upon our previous experience in designing Newton-conjugate-gradient methods for computing solitary waves and their linear-stability eigenvalues [2, 15], we now develop a method for computing time-periodic solutions which meet the above goals.

The main idea of this proposed method is the following. In view of the fact that the temporal period and possibly other additional parameters in the time-periodic solutions are unknown priori, our first step is to express those unknown parameters in terms of the solution through quasi-Rayleigh quotients, so that the resulting integro-differential equation is for the time-periodic solution only. Then this equation is solved in the combined spatiotemporal domain as a boundary value problem by the Newton-conjugate-gradient method, where Newton corrections are obtained by preconditioned conjugate-gradient iterations. The benefit of using conjugate-gradient iterations to solve the Newton-correction equation is two-fold: one is that it allows the computation to be performed entirely in the PDE framework (since these iterations apply to linear operator equations as well as matrix equations); and the other is that the power of conjugate-gradient iterations for solving large systems of linear equations can be brought out.

The proposed method applies to both stable and unstable time-periodic solutions; its numerical accuracy is spectral (since it is compatible with spectral differentiation [16, 17]), and its coding is short and simple. As numerical examples, this method is applied to the Kuramoto-Sivashinsky equation and the cubic-quintic Ginzburg-Landau equation, whose time-periodic or relative time-periodic solutions with spatially-periodic or spatially-localized profiles are computed. This method also applies to systems of ODEs, as is illustrated by its simple computation of periodic orbits in the Lorenz equations. These numerical examples reveal that the proposed method is very fast, as it only takes from a fraction of a second to a couple of minutes (on a personal computer) to find solutions of varying complexities to the accuracy of 10^{-10} . The simplicity of coding of the proposed method is evidenced in appendices, where stand-alone MATLAB codes for all numerical examples are provided.

II. A NUMERICAL METHOD FOR TIME-PERIODIC SOLUTIONS WITH AN UNKNOWN PERIOD ONLY

We first present a numerical method for computing time-periodic solutions whose temporal period is the only unknown parameter. For example, time-periodic solutions in the Kuramoto-Sivashinsky equation [18, 19]

$$u_t + uu_x + u_{xx} + \gamma u_{xxxx} = 0 \quad (1)$$

and the damped parametrically-driven nonlinear Schrödinger (NLS) equation [8]

$$i\psi_t + \psi_{xx} + 2|\psi|^2\psi - \psi = h\psi^* - i\gamma\psi \quad (2)$$

belong to this category. In the Kuramoto-Sivashinsky equation (1), $u(x, t)$ is a real variable and γ a real “superviscosity” coefficient. In the damped-forced NLS equation (2), $\psi(x, t)$ is a complex variable, and h, γ are real coefficients. Both equations admit solutions that are time-periodic, but the temporal period is not known priori and needs to be determined along with the solution itself [5, 6, 8, 20, 21].

Dissipative systems which admit time-periodic solutions with only an unknown temporal period can be cast in the following general form

$$\mathbf{u}_t = \mathbf{F}(\mathbf{x}, \partial_{\mathbf{x}}, \mathbf{u}), \quad (3)$$

where $\mathbf{x} = (x_1, x_2, \dots, x_N)$ is the N -dimensional spatial coordinate, $\mathbf{u}(\mathbf{x}, t)$ is a real-valued vector variable of \mathbf{x} and time t , and \mathbf{F} is a real-valued, generally nonlinear vector function of \mathbf{x} , \mathbf{u} and its spatial derivatives. Notice here that we allow \mathbf{F} to contain explicit dependence on \mathbf{x} (to incorporate spatial inhomogeneities), but not on time t . The Kuramoto-Sivashinsky equation (1) naturally falls into this general form, where $\mathbf{F}(\partial_x, u) = -(uu_x + u_{xx} + \gamma u_{xxx})$, which does not depend explicitly on x . The damped-forced NLS equation (2) falls into this general form as well when it is rewritten in terms of the real and imaginary parts of the complex function ψ (which make up the real vector variable \mathbf{u}).

Since Eq. (3) admits a time-periodic solution $\mathbf{u}(\mathbf{x}, t)$ with an unknown temporal period T , i.e., $\mathbf{u}(\mathbf{x}, t+T) = \mathbf{u}(\mathbf{x}, t)$, it proves convenient to introduce a time scaling

$$\tau = \omega t, \quad \omega \equiv 2\pi/T. \quad (4)$$

Under this scaling, Eq. (3) becomes

$$\omega \mathbf{u}_\tau = \mathbf{F}(\mathbf{x}, \partial_{\mathbf{x}}, \mathbf{u}), \quad (5)$$

where $\mathbf{u}(\mathbf{x}, \tau)$ is 2π -periodic in τ , i.e.,

$$\mathbf{u}(\mathbf{x}, \tau + 2\pi) = \mathbf{u}(\mathbf{x}, \tau). \quad (6)$$

Thus the computational domain for $\mathbf{u}(\mathbf{x}, \tau)$ can be set explicitly as $0 \leq \tau \leq 2\pi$ and $\mathbf{x} \in \Omega$, where Ω is the \mathbf{x} -domain of the solution $\mathbf{u}(\mathbf{x}, t)$. In the scaled equation (5), the frequency ω is the new unknown parameter.

To solve Eq. (5) with the temporal periodicity condition (6) and unknown frequency ω , our idea is to first express this unknown frequency ω in terms of the periodic solution $\mathbf{u}(\mathbf{x}, \tau)$ through a Rayleigh-like quotient. That is, we take the inner product of Eq. (5) with function \mathbf{u}_τ , and then obtain ω as

$$\omega = \frac{\langle \mathbf{u}_\tau, \mathbf{F} \rangle}{\langle \mathbf{u}_\tau, \mathbf{u}_\tau \rangle}. \quad (7)$$

Here the inner product is the standard one in the real-valued vector functional space

$$\langle \mathbf{f}(\mathbf{x}, \tau), \mathbf{g}(\mathbf{x}, \tau) \rangle = \int_0^{2\pi} \int_\Omega \mathbf{f}^\top \mathbf{g} \, d\mathbf{x} \, d\tau, \quad (8)$$

where the superscript ‘ \top ’ represents transpose of a vector. In this article, we call the Rayleigh-like quotient (7) as a quasi-Rayleigh quotient. Inserting this quasi-Rayleigh quotient (7) into (5), we then get the equation

$$\mathbb{L}_0(\mathbf{u}) \equiv \frac{\langle \mathbf{u}_\tau, \mathbf{F} \rangle}{\langle \mathbf{u}_\tau, \mathbf{u}_\tau \rangle} \mathbf{u}_\tau - \mathbf{F} = 0. \quad (9)$$

In this equation, the unknown frequency ω is gone, thus the equation is for the unknown function $\mathbf{u}(\mathbf{x}, \tau)$ only. The price to pay for this benefit is that this equation now becomes an integro-differential equation instead of a differential equation. But this is a price worth paying for.

We solve the integro-differential equation (9) by the Newton-conjugate-gradient (Newton-CG) method [2]. In this method, conjugate gradient (CG) iterations are used to solve the linear Newton-correction equation. Suppose $\mathbf{u}_n(\mathbf{x}, \tau)$ is the n -th approximation to the exact solution, then the Newton iteration for the next approximation is

$$\mathbf{u}_{n+1} = \mathbf{u}_n + \Delta \mathbf{u}_n, \quad (10)$$

where the linear Newton-correction equation for $\Delta \mathbf{u}_n$ is

$$\mathbf{L}_{1n} \Delta \mathbf{u}_n = -\mathbf{L}_0(\mathbf{u}_n). \quad (11)$$

Here \mathbf{L}_1 is the linearization operator of function $\mathbf{L}_0(\mathbf{u})$, i.e.,

$$\mathbf{L}_0(\mathbf{u} + \tilde{\mathbf{u}}) = \mathbf{L}_0(\mathbf{u}) + \mathbf{L}_1 \tilde{\mathbf{u}} + O(\tilde{\mathbf{u}}^2), \quad \tilde{\mathbf{u}} \ll 1, \quad (12)$$

and \mathbf{L}_{1n} is \mathbf{L}_1 evaluated at $\mathbf{u} = \mathbf{u}_n$. This linearization operator \mathbf{L}_1 is the counterpart of the Jacobian in systems of nonlinear ordinary differential equations.

Now we derive the analytical expression for \mathbf{L}_1 . Suppose the linearization operator for the function $\mathbf{F}(\mathbf{x}, \partial_{\mathbf{x}}, \mathbf{u})$ is \mathbf{F}_1 , i.e.,

$$\mathbf{F}(\mathbf{x}, \partial_{\mathbf{x}}, \mathbf{u} + \tilde{\mathbf{u}}) = \mathbf{F}(\mathbf{x}, \partial_{\mathbf{x}}, \mathbf{u}) + \mathbf{F}_1 \tilde{\mathbf{u}} + O(\tilde{\mathbf{u}}^2), \quad \tilde{\mathbf{u}} \ll 1. \quad (13)$$

When a dissipative wave system (3) is given, the function $\mathbf{F}(\mathbf{x}, \partial_{\mathbf{x}}, \mathbf{u})$ is known, thus its linearization operator \mathbf{F}_1 can be analytically obtained (this calculation for the Kuramoto-Sivashinsky equation (1) will be demonstrated in section IV). Using the linearization (13) for \mathbf{F} , the linearization for $\omega(\mathbf{u})$ in Eq. (7) is

$$\omega(\mathbf{u} + \tilde{\mathbf{u}}) = \frac{\langle (\mathbf{u} + \tilde{\mathbf{u}})_{\tau}, \mathbf{F}(\mathbf{x}, \partial_{\mathbf{x}}, \mathbf{u} + \tilde{\mathbf{u}}) \rangle}{\langle (\mathbf{u} + \tilde{\mathbf{u}})_{\tau}, (\mathbf{u} + \tilde{\mathbf{u}})_{\tau} \rangle} = \frac{\langle (\mathbf{u} + \tilde{\mathbf{u}})_{\tau}, \mathbf{F}(\mathbf{x}, \partial_{\mathbf{x}}, \mathbf{u}) + \mathbf{F}_1 \tilde{\mathbf{u}} \rangle}{\langle (\mathbf{u} + \tilde{\mathbf{u}})_{\tau}, (\mathbf{u} + \tilde{\mathbf{u}})_{\tau} \rangle} + O(\tilde{\mathbf{u}}^2).$$

Utilizing Eq. (5), we get

$$\omega(\mathbf{u} + \tilde{\mathbf{u}}) = \frac{\langle (\mathbf{u} + \tilde{\mathbf{u}})_{\tau}, \omega(\mathbf{u}) \mathbf{u}_{\tau} + \mathbf{F}_1 \tilde{\mathbf{u}} \rangle}{\langle (\mathbf{u} + \tilde{\mathbf{u}})_{\tau}, (\mathbf{u} + \tilde{\mathbf{u}})_{\tau} \rangle} + O(\tilde{\mathbf{u}}^2) = \frac{\langle (\mathbf{u} + \tilde{\mathbf{u}})_{\tau}, \omega(\mathbf{u}) (\mathbf{u} + \tilde{\mathbf{u}})_{\tau} - [\omega(\mathbf{u}) \partial_{\tau} - \mathbf{F}_1] \tilde{\mathbf{u}} \rangle}{\langle (\mathbf{u} + \tilde{\mathbf{u}})_{\tau}, (\mathbf{u} + \tilde{\mathbf{u}})_{\tau} \rangle} + O(\tilde{\mathbf{u}}^2),$$

thus

$$\omega(\mathbf{u} + \tilde{\mathbf{u}}) = \omega(\mathbf{u}) - \frac{\langle \mathbf{u}_{\tau}, [\omega(\mathbf{u}) \partial_{\tau} - \mathbf{F}_1] \tilde{\mathbf{u}} \rangle}{\langle \mathbf{u}_{\tau}, \mathbf{u}_{\tau} \rangle} + O(\tilde{\mathbf{u}}^2). \quad (14)$$

Using this $\omega(\mathbf{u})$ linearization as well as the $\mathbf{F}(\mathbf{x}, \partial_{\mathbf{x}}, \mathbf{u})$ linearization (13), the linearization operator \mathbf{L}_1 for $\mathbf{L}_0(\mathbf{u})$ can then be found as

$$\mathbf{L}_1 \Psi = \mathbf{P} \Psi - \frac{\langle \mathbf{u}_{\tau}, \mathbf{P} \Psi \rangle}{\langle \mathbf{u}_{\tau}, \mathbf{u}_{\tau} \rangle} \mathbf{u}_{\tau}, \quad (15)$$

where

$$\mathbf{P} \equiv \omega \partial_{\tau} - \mathbf{F}_1, \quad (16)$$

and $\omega(\mathbf{u})$ is given through \mathbf{u} by the quasi-Rayleigh quotient (7).

It is now time to discuss how to solve the linear Newton-correction equation (11). In the Newton-CG method, this equation will be solved by conjugate-gradient iterations, which is widely recognized as probably the fastest way to solve large systems of linear inhomogeneous equations [14]. Since the homogeneous operator \mathbf{L}_1 in (15) is apparently non-self-adjoint, it is necessary to turn equation (11) into a sort of normal equation so that its homogeneous operator becomes self-adjoint. The usual way to turn (11) into a normal equation is to multiply it by the adjoint operator of \mathbf{L}_1 . But due to the special structure of \mathbf{L}_1 in (15), we can “cut corners” and just multiply (11) by the adjoint operator of \mathbf{P} , which is

$$\mathbf{P}^A = -\omega \partial_{\tau} - \mathbf{F}_1^A, \quad (17)$$

where \mathbf{F}_1^A is the adjoint operator of \mathbf{F}_1 . Here the superscript ‘A’ represents the adjoint. With this multiplication, the Newton-correction equation (11) becomes

$$\mathbf{P}_n^A \mathbf{L}_{1n} \Delta \mathbf{u}_n = -\mathbf{P}_n^A \mathbf{L}_0(\mathbf{u}_n), \quad (18)$$

where \mathbf{P}_n^A is \mathbf{P}^A evaluated at $\mathbf{u} = \mathbf{u}_n$. For convenience, we call this equation a quasi-normal equation. It is easy to check that $\mathbf{P}^A \mathbf{L}_1$ is self-adjoint. In addition, using the Cauchy-Schwarz inequality, we can show that $\mathbf{P}^A \mathbf{L}_1$ is also semi-positive definite. Thus the quasi-normal equation (18) can be solved by preconditioned conjugate gradient iterations. The numerical algorithm for preconditioned conjugate gradient iterations is well known [14] and will not be repeated here (the reader can refer to the sample MATLAB codes in the appendices for numerical executions of these iterations). We do want to mention that, in order to avoid over-solving, CG iterations for the quasi-normal equation (18) will be stopped when the error of the Newton-correction solution $\Delta \mathbf{u}_n$ drops below a certain fraction of the error of the solution \mathbf{u}_n itself [15] (in our coding, this fraction is set as `errorCG`= 10^{-4} , see appendices). This strategy reduces the number of CG iterations for solving each Newton-correction equation at the expense of losing the quadratic convergence of Newton iterations, but its benefit outweighs its price [15].

To summarize, our numerical algorithm for computing time-periodic solutions $\mathbf{u}(\mathbf{x}, t)$ with unknown temporal periods in Eq. (3) is:

1. turn (3) into an integro-differential equation (9) for the function $\mathbf{u}(\mathbf{x}, \tau)$ only, under the time-periodic boundary condition (6);
2. solve (9) by Newton iterations

$$\mathbf{u}_{n+1} = \mathbf{u}_n + \Delta \mathbf{u}_n,$$

where Newton corrections $\Delta \mathbf{u}_n$ are computed from the quasi-normal equation

$$\mathbf{P}_n^A \mathbf{L}_{1n} \Delta \mathbf{u}_n = -\mathbf{P}_n^A \mathbf{L}_0(\mathbf{u}_n)$$

by preconditioned conjugate gradient iterations. Here, linear operators \mathbf{L}_1 and \mathbf{P}^A are given analytically by equations (15)-(17);

3. after $\mathbf{u}(\mathbf{x}, \tau)$ is obtained, the temporal period $T(= 2\pi/\omega)$ is then derived from the quasi-Rayleigh quotient (7).

The above numerical algorithm is attractive for a number of reasons. First the entire computation is performed in the PDE framework (no truncation to ODEs or algebraic equations is necessary). Second, it is applicable to both stable and unstable time-periodic solutions. This contrasts the time-evolution method which can only converge to stable solutions. Thirdly, its numerical accuracy can be very high. Indeed, if we use the discrete Fourier transform or Chebyshev differentiation to compute all spatial and temporal derivatives, then its numerical accuracy would be spectral [16, 17]. Fourthly, this method is fast-converging and very efficient. This efficiency will be illustrated on several numerical examples in section IV, where we will see that this method only takes from a fraction of a second to a couple of minutes (on a personal computer) to find solutions of varying complexities to the accuracy of 10^{-10} . Fifthly, the coding of this method is very short and compact, as is evidenced in the sample MATLAB codes to be presented in the appendices.

In the implementation of the above Newton-CG method, there are two practical issues. One is the choice of the preconditioning operator for solving the quasi-normal equation by preconditioned conjugate gradient iterations. This preconditioner, say \mathbf{M} , must be self-adjoint and positive definite. In addition, it should make the condition number of $\mathbf{M}^{-1} \mathbf{P}^A \mathbf{L}_1$ as small as possible (i.e., to make $\mathbf{M}^{-1} \mathbf{P}^A \mathbf{L}_1$ as close to the identity operator as possible) in order to get faster convergence. Furthermore it should be easy to invert, since this inversion is needed during iterations. Since the large condition number of $\mathbf{P}^A \mathbf{L}_1$ in the quasi-normal equation, which slows down CG iterations, is generally caused by higher space and time derivatives in $\mathbf{P}^A \mathbf{L}_1$, then a general guideline for the choice of the preconditioner is to retain only the higher-derivative terms in $\mathbf{P}^A \mathbf{L}_1$ and use the resulting operator as \mathbf{M} (added by a positive constant to make \mathbf{M} positive-definite). Implementation of this guideline on several numerical examples will be illustrated in section IV.

The other practical issue in the Newton-CG method is the choice of the initial condition. It is well known that if the initial condition is not properly chosen, Newton iterations may not converge. There are various strategies for choosing the initial condition. The first strategy is to just choose the initial condition randomly. This strategy may

work, especially if the solution has a simple structure, but one often needs to try many initial conditions in order to hit upon one that works. A second strategy is to simulate the time evolution of the original wave equation and inspect the solution to see if any time-segment of this solution is close to time-periodic or not. If so, then that time-segment of the solution will be used as our initial condition for Newton-CG iterations. Note that this second strategy is applicable to both stable and unstable time-periodic solutions, since even if the solution is unstable, time evolution of the wave equation may still get close to this solution and wander around it for a little while (before veering off), and that approximate time-periodic segment is often sufficient as our initial condition for Newton-CG iterations. A third strategy is by continuation. If we have obtained a time-periodic solution at one parameter value, then by continuously changing this parameter and using the previous solution as the initial condition, we can trace a whole family of time-periodic solutions for a continuous range of this parameter. This continuation strategy is often very useful, especially for studying bifurcations of solutions as parameters vary. In our numerical examples of section IV, we will apply all these strategies to select initial conditions of Newton-CG iterations for both stable and unstable time-periodic solutions.

III. A NUMERICAL METHOD FOR TIME-PERIODIC SOLUTIONS WITH MULTIPLE UNKNOWN PARAMETERS

In some dissipative wave systems, time-periodic solutions have more unknown parameters than just the temporal period. One example is the Ginzburg-Landau-type equations such as

$$A_t = \chi A + \gamma A_{xx} - \beta |A|^2 A - \delta |A|^4 A, \quad (19)$$

where A is a complex variable, and $\chi, \gamma, \beta, \delta$ are complex coefficients. This equation does not admit truly time-periodic solutions, but it admits the so-called relative time-periodic solutions of the form

$$A(x, t) = e^{i\mu t} U(x, t), \quad (20)$$

where $U(x, t)$ is a time-periodic complex function, and μ is a real-valued propagation constant [7, 22, 23]. In this solution, both the temporal period T of $U(x, t)$ and the propagation constant μ are unknown in addition to the unknown function $U(x, t)$. In order to compute these relative time-periodic solutions, the numerical algorithm of the previous section needs to be modified and generalized.

In this section, we develop a numerical scheme to compute time-periodic solutions with multiple unknown parameters (here ‘time-periodic solutions’ is interpreted in the broader sense, including relative time-periodic solutions). The basic idea is similar to that of the previous section. That is, we first express these unknown parameters in terms of the time-periodic function through quasi-Rayleigh quotients so that the original wave equation becomes an integro-differential equation for the unknown time-periodic function only. Then we use Newton-CG iterations to solve this integro-differential equation. But since the current problem involves multiple unknown parameters, the linearization operator of the integro-differential equation will have a different structure than Eq. (15) of the previous section. Because of that, we will have to solve the linear Newton-correction equation (through CG iterations) by turning it into a true normal equation instead of a quasi-normal equation. That is, we will need to multiply the Newton-correction equation by the adjoint of the whole Newton-linearization operator rather than a partial one.

Even though our basic idea for computing time-periodic solutions with multiple unknown parameters is easy to state, formulation of this idea for general dissipative systems can be cumbersome. Thus in the following, we only formulate this idea for a special (but important) class of equations, namely the Ginzburg-Landau-type equations. Extension of this formulation to other types of equations is straightforward.

The class of Ginzburg-Landau-type equations that we consider can be written in the following general form,

$$A_t = f(|A|, \mathbf{x}, \partial_{\mathbf{x}})A, \quad (21)$$

where $\mathbf{x} = (x_1, x_2, \dots, x_N)$ is the N -dimensional spatial coordinate, $A(\mathbf{x}, t)$ is a complex-valued scalar variable of \mathbf{x} and time t , and f is a complex-valued function of $|A|$, \mathbf{x} and the spatial derivatives. As before, we allow f to contain explicit dependence on \mathbf{x} (to model spatial inhomogeneities), but not on time t . The cubic-quintic Ginzburg-Landau equation (19) is an example of this general form, with $f(|A|, \partial_x) = \chi + \gamma \partial_{xx} - \beta |A|^2 - \delta |A|^4$, which contains no explicit x -dependence.

This class of Ginzburg-Landau-type equations admit relative time-periodic solutions of the form

$$A(\mathbf{x}, t) = e^{i\mu t} U(\mathbf{x}, t), \quad (22)$$

where $U(\mathbf{x}, t)$ is a time-periodic complex function, and μ is a real-valued propagation constant. These solutions can be spatially localized or periodic [7, 22, 23]. Both the temporal period T and the propagation constant μ are not known priori and must be determined along with the time-periodic function $U(\mathbf{x}, t)$.

Substituting (22) into Eq. (21), we get the equation for the time-periodic function $U(\mathbf{x}, t)$ as

$$U_t + i\mu U = G, \quad (23)$$

where

$$G \equiv f(|U|, \mathbf{x}, \partial_{\mathbf{x}})U. \quad (24)$$

As before, we employ a time scaling

$$\tau = \omega t, \quad \omega \equiv 2\pi/T, \quad (25)$$

where T is the temporal period of the function $U(\mathbf{x}, t)$. Under this scaling, Eq. (23) becomes

$$\omega U_{\tau} + i\mu U = G, \quad (26)$$

where $U(\mathbf{x}, \tau)$ is 2π -periodic in τ , i.e.,

$$U(\mathbf{x}, \tau + 2\pi) = U(\mathbf{x}, \tau). \quad (27)$$

Thus the computational domain for $U(\mathbf{x}, \tau)$ will be set explicitly as $0 \leq \tau \leq 2\pi$ and $\mathbf{x} \in \Omega$, where Ω is the \mathbf{x} -domain of the solution $U(\mathbf{x}, t)$.

To solve Eq. (26), we first express the unknown real parameters ω and μ in terms of $U(\mathbf{x}, \tau)$ through quasi-Rayleigh quotients. For this purpose, it is convenient to split the complex functions U and G into real and imaginary parts as

$$U = u + iv, \quad G = g + ih. \quad (28)$$

Inserting this split into Eq. (26), equations for the real and imaginary parts u, v of the solution can be readily obtained as

$$\omega u_{\tau} - \mu v - g = 0, \quad (29)$$

$$\omega v_{\tau} + \mu u - h = 0. \quad (30)$$

Taking inner products of these equations with u, v, u_{τ}, v_{τ} , adding or subtracting the resulting equations, and utilizing the τ -periodicity of (u, v) , parameters μ and ω can be expressed through the following quasi-Rayleigh quotients,

$$\mu = \frac{\langle v, h \rangle - \langle u, g \rangle}{2\langle u, v \rangle}, \quad \omega = \frac{\langle u_{\tau}, h \rangle + \langle v_{\tau}, g \rangle}{2\langle u_{\tau}, v_{\tau} \rangle}. \quad (31)$$

Here the inner product is the same as that defined in Eq. (8). Inserting these quasi-Rayleigh quotients into (29)-(30), these equations then become the following integro-differential equations for the unknown functions $\mathbf{u} \equiv [u, v]^T$ only,

$$\mathbf{L}_0(\mathbf{u}) \equiv \begin{bmatrix} \omega u_{\tau} - \mu v - g \\ \omega v_{\tau} + \mu u - h \end{bmatrix} = 0, \quad (32)$$

where $\mu(\mathbf{u})$ and $\omega(\mathbf{u})$ are given in equation (31).

We use Newton-CG methods to solve the integro-differential equations (32). As before, the Newton iterations are

$$\mathbf{u}_{n+1} = \mathbf{u}_n + \Delta \mathbf{u}_n, \quad (33)$$

where the linear Newton-correction equation for $\Delta \mathbf{u}_n$ is

$$\mathbf{L}_{1n} \Delta \mathbf{u}_n = -\mathbf{L}_0(\mathbf{u}_n), \quad (34)$$

and \mathbf{L}_1 is the linearization operator of function $\mathbf{L}_0(\mathbf{u})$. The key question now is the analytical expression for this linearization operator, which is certainly different from (15) of the previous section. This expression of \mathbf{L}_1 is given in the following lemma.

Lemma 1 The linearization operator \mathbf{L}_1 of $\mathbf{L}_0(\mathbf{u})$ in Eq. (32) is

$$\mathbf{L}_1 \Psi = \mathbf{P} \Psi - \frac{\left\langle \begin{bmatrix} v_\tau \\ u_\tau \end{bmatrix}, \mathbf{P} \Psi \right\rangle}{2\langle u_\tau, v_\tau \rangle} \begin{bmatrix} u_\tau \\ v_\tau \end{bmatrix} + \frac{\left\langle \begin{bmatrix} u \\ -v \end{bmatrix}, \mathbf{P} \Psi \right\rangle}{2\langle u, v \rangle} \begin{bmatrix} -v \\ u \end{bmatrix}, \quad (35)$$

where

$$\mathbf{P} = \begin{bmatrix} \omega \partial_\tau & -\mu \\ \mu & \omega \partial_\tau \end{bmatrix} - \mathbf{G}_1, \quad (36)$$

and \mathbf{G}_1 is the linearization operator of the vector function $[g, h]^T$, i.e.,

$$\begin{bmatrix} g(u + \tilde{u}, v + \tilde{v}) \\ h(u + \tilde{u}, v + \tilde{v}) \end{bmatrix} = \begin{bmatrix} g(u, v) \\ h(u, v) \end{bmatrix} + \mathbf{G}_1 \begin{bmatrix} \tilde{u} \\ \tilde{v} \end{bmatrix} + O(\tilde{u}^2, \tilde{u}\tilde{v}, \tilde{v}^2). \quad (37)$$

The proof of this lemma will be provided later in this section. For the example of the cubic-quintic Ginzburg-Landau equation (19), calculation of the linear operator \mathbf{G}_1 will be illustrated in section IV.

We can notice that the linearization operator \mathbf{L}_1 in this lemma has a more complex structure than that in (15) of the previous section. Because of that, in order to turn \mathbf{L}_1 into a self-adjoint operator, we have to multiply it by its full adjoint \mathbf{L}_1^A . In other words, in order to solve the linear Newton-correction equation (34) by conjugate gradient iterations, we need to turn it into the usual normal equation

$$\mathbf{L}_{1n}^A \mathbf{L}_{1n} \Delta \mathbf{u}_n = -\mathbf{L}_{1n}^A \mathbf{L}_0(\mathbf{u}_n). \quad (38)$$

Compared with the previous quasi-normal equation (18), we have no ‘‘corners to cut’’ here. Obviously the linear operator $\mathbf{L}_{1n}^A \mathbf{L}_{1n}$ in the above normal equation is self-adjoint and semi-positive definite, thus this equation can be solved effectively by preconditioned conjugate gradient iterations.

The normal equation (38) involves the adjoint operator \mathbf{L}_1^A . This adjoint operator can be derived from \mathbf{L}_1 in Lemma 1, and its analytical expression is provided by the following lemma.

Lemma 2 The adjoint operator of \mathbf{L}_1 in Lemma 1 is

$$\mathbf{L}_1^A \Psi = \mathbf{P}^A \Psi - \frac{\left\langle \Psi, \begin{bmatrix} u_\tau \\ v_\tau \end{bmatrix} \right\rangle}{2\langle u_\tau, v_\tau \rangle} \mathbf{P}^A \begin{bmatrix} v_\tau \\ u_\tau \end{bmatrix} + \frac{\left\langle \Psi, \begin{bmatrix} -v \\ u \end{bmatrix} \right\rangle}{2\langle u, v \rangle} \mathbf{P}^A \begin{bmatrix} u \\ -v \end{bmatrix}, \quad (39)$$

where

$$\mathbf{P}^A = \begin{bmatrix} -\omega \partial_\tau & \mu \\ -\mu & -\omega \partial_\tau \end{bmatrix} - \mathbf{G}_1^A \quad (40)$$

is the adjoint operator of \mathbf{P} , and \mathbf{G}_1^A is the adjoint operator of \mathbf{G}_1 .

The proof for this lemma will follow shortly.

To summarize, our numerical algorithm for computing relative time-periodic solutions (22), with unknown temporal period T and propagation constant μ , in the class of Ginzburg-Landau-type equations (21) is

1. turn (21) into an integro-differential equation (32) for the real and imaginary parts $\mathbf{u} \equiv [u, v]^T$ of the solution $U(\mathbf{x}, \tau)$ only, under the time-periodic boundary condition (27);

2. solve (32) by Newton iterations

$$\mathbf{u}_{n+1} = \mathbf{u}_n + \Delta \mathbf{u}_n,$$

where Newton corrections $\Delta \mathbf{u}_n$ are computed from the normal equation

$$\mathbf{L}_{1n}^A \mathbf{L}_{1n} \Delta \mathbf{u}_n = -\mathbf{L}_{1n}^A \mathbf{L}_0(\mathbf{u}_n)$$

by preconditioned conjugate gradient iterations. Here, linear operators \mathbf{L}_1 and \mathbf{L}_1^A are given analytically in Lemmas 1 and 2.

3. after $\mathbf{u}(\mathbf{x}, \tau)$ is obtained, the temporal period $T(= 2\pi/\omega)$ and the propagation constant μ are then calculated from the quasi-Rayleigh quotients (31).

This numerical method shares the same attractive features as that described in the previous section (such as high accuracy, efficiency, short coding, and so on). In the implementation of this method, we also face the two practical issues discussed in the end of section 2, which are choices of the preconditioner and the initial condition. Our guidelines for these choices are the same as those spelled out there.

Now we prove Lemmas 1 and 2.

Proof of Lemma 1. We first derive linearizations for the quasi-Rayleigh quotients of μ and ω . For this purpose, we rewrite the μ formula as

$$\mu(u, v) = \frac{\left\langle \begin{bmatrix} -u \\ v \end{bmatrix}, \begin{bmatrix} g(u, v) \\ h(u, v) \end{bmatrix} \right\rangle}{2\langle u, v \rangle}.$$

Utilizing the linearization (37) for $[g, h]^T$, we get

$$\mu(u + \tilde{u}, v + \tilde{v}) = \frac{\left\langle \begin{bmatrix} -(u + \tilde{u}) \\ v + \tilde{v} \end{bmatrix}, \begin{bmatrix} g(u, v) \\ h(u, v) \end{bmatrix} + \mathbf{G}_1 \begin{bmatrix} \tilde{u} \\ \tilde{v} \end{bmatrix} \right\rangle}{2\langle u + \tilde{u}, v + \tilde{v} \rangle} + O(\tilde{u}^2, \tilde{u}\tilde{v}, \tilde{v}^2).$$

Then using equations (29)-(30), we can calculate $\mu(u + \tilde{u}, v + \tilde{v})$ as

$$\begin{aligned} \mu(u + \tilde{u}, v + \tilde{v}) &= \frac{\left\langle \begin{bmatrix} -(u + \tilde{u}) \\ v + \tilde{v} \end{bmatrix}, \begin{bmatrix} \omega u_\tau - \mu v \\ \omega v_\tau + \mu u \end{bmatrix} + \mathbf{G}_1 \begin{bmatrix} \tilde{u} \\ \tilde{v} \end{bmatrix} \right\rangle}{2\langle u + \tilde{u}, v + \tilde{v} \rangle} + O(\tilde{u}^2, \tilde{u}\tilde{v}, \tilde{v}^2) \\ &= \frac{\left\langle \begin{bmatrix} -(u + \tilde{u}) \\ v + \tilde{v} \end{bmatrix}, \omega \begin{bmatrix} u + \tilde{u} \\ v + \tilde{v} \end{bmatrix}_\tau + \mu \begin{bmatrix} -(v + \tilde{v}) \\ u + \tilde{u} \end{bmatrix} - \mathbf{P} \begin{bmatrix} \tilde{u} \\ \tilde{v} \end{bmatrix} \right\rangle}{2\langle u + \tilde{u}, v + \tilde{v} \rangle} + O(\tilde{u}^2, \tilde{u}\tilde{v}, \tilde{v}^2), \end{aligned}$$

where μ, ω on the right sides of these equations are abbreviations for $\mu(u, v), \omega(u, v)$, and operator \mathbf{P} is as defined in (36). Recalling the τ -periodicity of functions $u + \tilde{u}$ and $v + \tilde{v}$, the above expression for $\mu(u + \tilde{u}, v + \tilde{v})$ can be simplified as

$$\mu(u + \tilde{u}, v + \tilde{v}) = \mu(u, v) - \frac{\left\langle \begin{bmatrix} -u \\ v \end{bmatrix}, \mathbf{P} \begin{bmatrix} \tilde{u} \\ \tilde{v} \end{bmatrix} \right\rangle}{2\langle u, v \rangle} + O(\tilde{u}^2, \tilde{u}\tilde{v}, \tilde{v}^2),$$

which is the linearization for the quasi-Rayleigh quotient of μ . Performing similar calculations, the linearization for the quasi-Rayleigh quotient of ω is found as

$$\omega(u + \tilde{u}, v + \tilde{v}) = \omega(u, v) - \frac{\left\langle \begin{bmatrix} v_\tau \\ u_\tau \end{bmatrix}, \mathbf{P} \begin{bmatrix} \tilde{u} \\ \tilde{v} \end{bmatrix} \right\rangle}{2\langle u_\tau, v_\tau \rangle} + O(\tilde{u}^2, \tilde{u}\tilde{v}, \tilde{v}^2).$$

Using these linearizations of μ and ω as well as the linearization (37) of $[g, h]^T$, the linearization operator L_1 for equation (32) is then found to be (35) in Lemma 1.

Proof of Lemma 2. The definition for adjoint operators is that

$$\langle \Phi, L_1 \Psi \rangle = \langle L_1^A \Phi, \Psi \rangle.$$

Using the expression of L_1 in Lemma 1 as well as the basic relation of $\langle \Phi, P\Psi \rangle = \langle P^A \Phi, \Psi \rangle$, we find that

$$\begin{aligned} \langle \Phi, L_1 \Psi \rangle &= \langle \Phi, P\Psi \rangle - \frac{\left\langle \begin{bmatrix} v_\tau \\ u_\tau \end{bmatrix}, P\Psi \right\rangle \left\langle \Phi, \begin{bmatrix} u_\tau \\ v_\tau \end{bmatrix} \right\rangle}{2\langle u_\tau, v_\tau \rangle} + \frac{\left\langle \begin{bmatrix} u \\ -v \end{bmatrix}, P\Psi \right\rangle \left\langle \Phi, \begin{bmatrix} -v \\ u \end{bmatrix} \right\rangle}{2\langle u, v \rangle} \\ &= \langle P^A \Phi, \Psi \rangle - \frac{\left\langle \Phi, \begin{bmatrix} u_\tau \\ v_\tau \end{bmatrix} \right\rangle \left\langle P^A \begin{bmatrix} v_\tau \\ u_\tau \end{bmatrix}, \Psi \right\rangle}{2\langle u_\tau, v_\tau \rangle} + \frac{\left\langle \Phi, \begin{bmatrix} -v \\ u \end{bmatrix} \right\rangle \left\langle P^A \begin{bmatrix} u \\ -v \end{bmatrix}, \Psi \right\rangle}{2\langle u, v \rangle}, \end{aligned}$$

which is the same as $\langle L_1^A \Phi, \Psi \rangle$ with L_1^A given in Lemma 2.

To prove P^A in equation (40) is the adjoint operator of P , we only need to use the definition of adjoint operators, together with integration by parts and the fact that all admissible functions are τ -periodic.

Before concluding this section, we would like to make a remark. As the reader may notice, the expressions of μ and ω through quasi-Rayleigh quotients are not unique. Indeed, from equations (29)-(30) we can also derive other quasi-Rayleigh quotients of μ and ω different from (31). For instance, by taking the inner products of (29) with u and (30) with u_τ , and utilizing the τ -periodicity of the involved functions, we can obtain the following alternative expressions

$$\mu = -\frac{\langle u, g \rangle}{\langle u, v \rangle}, \quad \omega = \frac{\langle u_\tau, h \rangle}{\langle u_\tau, v_\tau \rangle}.$$

Substituting these alternative quasi-Rayleigh quotients into equations (29)-(30), we can still use Newton-CG iterations to solve them, except that the linearization operator L_1 and its adjoint L_1^A will be different from those in Lemmas 1 and 2. We have implemented this and several other versions of quasi-Rayleigh quotients on the cubic-quintic Ginzburg-Landau equation (19), and found that their performances are slightly inferior to the quasi-Rayleigh quotients in equation (31). The reason is probably that μ and ω in formulae (31) are derived by taking the average of inner products from equations (29) and (30). This averaging may give more accurate approximations for μ and ω from an approximate solution (u_n, v_n) , thus rendering the numerical scheme superior to some other alternatives.

IV. NUMERICAL EXAMPLES

In this section, we apply the proposed numerical methods of previous sections to three well-known dissipative systems, the Kuramoto-Sivashinsky equation, the cubic-quintic Ginzburg-Landau equation, and the Lorenz equations. Both stable and unstable time-periodic solutions in these equations will be computed. All our computations are performed in MATLAB on a Desktop PC (Dell Optiplex 990 with CPU speed 3.3GHz). MATLAB codes for these computations can be found in the appendices.

Example 1 Our first example is the Kuramoto-Sivashinsky (KS) equation (1), i.e.,

$$u_t + uu_x + u_{xx} + \gamma u_{xxx} = 0, \tag{41}$$

where u is a scalar real variable, and γ is a real ‘‘superviscosity’’ coefficient. This equation was derived in various physical contexts as a model for wave dynamics near long-wave-length instabilities in the presence of certain symmetries [18, 19, 24]. But it is also used to study spatiotemporal complexity [5, 6, 20, 21, 25]. In these studies, it is customary to impose the periodic boundary condition

$$u(x + 2\pi, t) = u(x, t). \tag{42}$$

Under this boundary condition, we seek time-periodic solutions in this equation. Thus the numerical domain of our algorithm will be set as $0 \leq x, \tau \leq 2\pi$. Since the only unknown parameter in these solutions is the temporal period, the algorithm in section 2 will be suitable. This algorithm is capable of obtaining both stable and unstable time-periodic solutions. Below we will apply it to determine unstable solutions, since such solutions cannot be obtained by the time-evolution method and are thus more challenging to find.

For the KS equation (41), the function \mathbf{F} in the algorithm of section 2 is

$$\mathbf{F}(\partial_x, u) = -(uu_x + u_{xx} + \gamma u_{xxxx}).$$

Linearization of this function is

$$\begin{aligned} \mathbf{F}(\partial_x, u + \tilde{u}) &= -[(u + \tilde{u})(u + \tilde{u})_x + (u + \tilde{u})_{xx} + \gamma(u + \tilde{u})_{xxxx}] \\ &= \mathbf{F}(\partial_x, u) - [u\partial_x + u_x + \partial_{xx} + \gamma\partial_{xxxx}] \tilde{u} + O(\tilde{u}^2), \end{aligned}$$

thus the linearization operator of \mathbf{F} is

$$\mathbf{F}_1 = -[u\partial_x + u_x + \partial_{xx} + \gamma\partial_{xxxx}].$$

Its adjoint operator \mathbf{F}_1^A can be easily derived from the basic condition $\langle \phi, \mathbf{F}_1 \psi \rangle = \langle \mathbf{F}_1^A \phi, \psi \rangle$ as

$$\mathbf{F}_1^A = -[-u\partial_x + \partial_{xx} + \gamma\partial_{xxxx}].$$

Using these formulae, the quasi-normal Newton-correction equation (18) for the KS equation is

$$\mathbf{P}_n^A \mathbf{L}_{1n} \Delta u_n = -\mathbf{P}_n^A \mathbf{L}_0(u_n), \quad (43)$$

where

$$\mathbf{L}_0(u) = \omega u_\tau - \mathbf{F}, \quad \mathbf{L}_1 \psi \equiv \mathbf{P} \psi - \frac{\langle u_\tau, \mathbf{P} \psi \rangle}{\langle u_\tau, u_\tau \rangle} u_\tau, \quad \mathbf{P} = \omega \partial_\tau - \mathbf{F}_1, \quad \mathbf{P}^A = -\omega \partial_\tau - \mathbf{F}_1^A, \quad \omega = \frac{\langle u_\tau, \mathbf{F} \rangle}{\langle u_\tau, u_\tau \rangle},$$

and the quantities with subscript ‘ n ’ in (43) are the corresponding quantities evaluated at the n -th approximate solution u_n .

Regarding the preconditioner \mathbf{M} in preconditioned conjugate gradient iterations on the quasi-normal equation (43), we take

$$\mathbf{M} = c - \omega^2 \partial_{\tau\tau} + (\partial_{xx} + \gamma \partial_{xxxx})^2,$$

where c is a positive constant (which we choose as $c = 30$; other c values deliver comparable performances). Our choice of this preconditioner follows the guidelines at the end of section 2. Specifically, neglecting lower-derivative terms in $\mathbf{P}^A \mathbf{L}_1$, we get

$$\mathbf{P}^A \mathbf{L}_1 \approx -\omega^2 \partial_{\tau\tau} + (\partial_{xx} + \gamma \partial_{xxxx})^2.$$

Since the preconditioner must be positive definite, it is sensible to add a positive constant to the above approximation and hence choose \mathbf{M} as above. Notice that this \mathbf{M} is self-adjoint (as required). In addition, its inversion is very simple by using the Fourier transform. The frequency ω in this preconditioner is given through the quasi-Rayleigh quotient in the equation below (43).

We first look for time-periodic solutions in the KS equation (41) with $\gamma = 0.054$. At this γ value, the KS equation admits an unstable time-periodic solution [25]. After many random trials (the first strategy described in the last paragraph of section 2), we arrive at a successful initial condition

$$u_0(x, \tau) = -7 \sin 3x - 3(\sin 4x - \sin 5x) \sin \tau - \sin x \cos \tau, \quad 0 \leq x, \tau \leq 2\pi. \quad (44)$$

In our Newton-CG iterations, we use 64 evenly-spaced grid points along each of the x and τ directions. Due to the periodic conditions of $u(x, \tau)$, we use the discrete (fast) Fourier transform to evaluate all spatial and temporal derivatives, which gives spectral accuracy for this algorithm [16, 17]. Due to this spectral accuracy, we find that 64 grid

points are already sufficient to yield solutions accurate within 10^{-10} . The MATLAB code of this algorithm is provided in Appendix A (this code is also posted at the author’s homepage: www.cems.uvm.edu/~jxyang/codes.htm).

The numerical result of this MATLAB code is displayed in Fig. 1. In panel (a), the initial condition (44) is shown (for two τ periods). From this initial condition, the accurate time-periodic solution obtained by the Newton-CG method is displayed in panel (b) for two periods of real time t , and the accurate period is found to be $T = 1.3297045458$. As one can see from these two panels, our initial condition differs significantly from the accurate solution, but the iteration still converges, meaning that the attraction basin of our Newton-CG method is quite large. Convergence speed of these Newton-CG iterations is displayed in the lower panels, where the error versus the number of CG iterations is plotted in panel (c), while the error versus the time spent is plotted in panel (d). The error here is defined as $\max|L_0(u_n)|$, i.e., maximum magnitude of the equation’s residue $L_0(u_n)$ at the numerical solution u_n . Panel (c) shows that this error drops from the initial value of about 300 to the final value of 10^{-10} under 5000 CG iterations, while panel (d) shows that this drop of the error from 300 to 10^{-10} takes about 6 seconds.

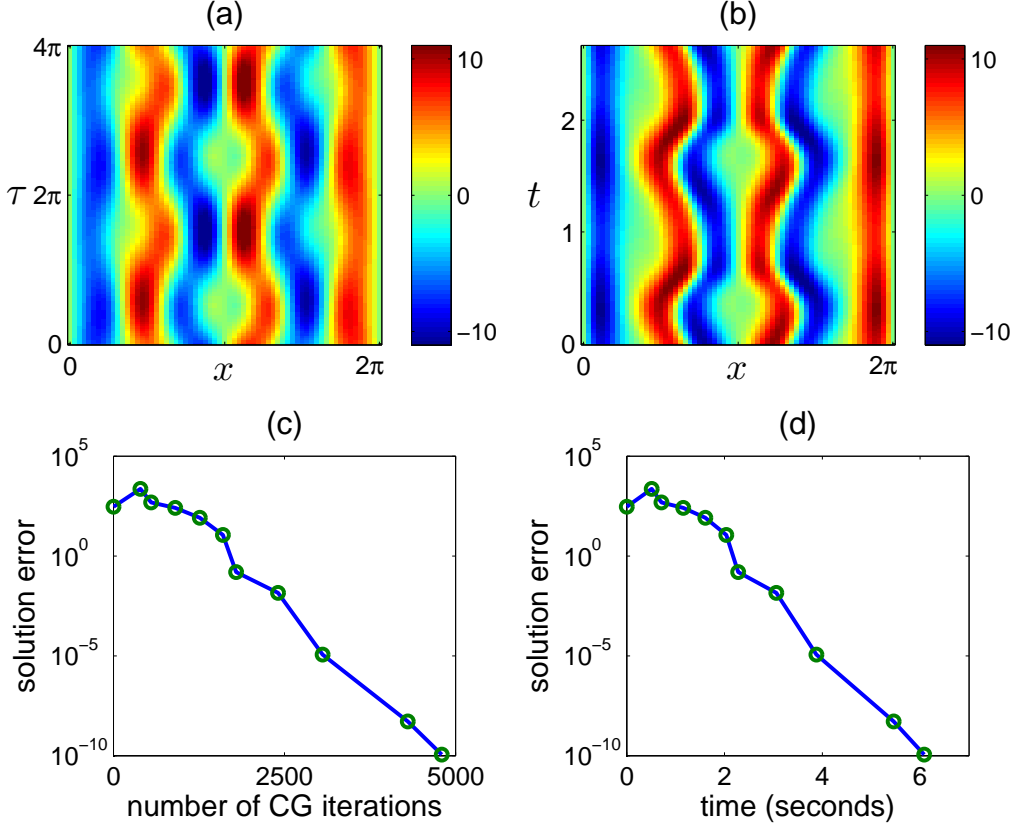


FIG. 1: Numerical computation of the time-periodic solution in the KS equation (41) at $\gamma = 0.054$. (a) The initial condition $u_0(x, \tau)$ in (44). (b) The accurate solution $u(x, t)$. (c) The graph of error versus number of CG iterations. (d) The graph of error versus the time spent. In (a, b), two time periods are shown. In (c, d), circles are Newton-iteration points. This figure is produced by the MATLAB code in Appendix A.

As the γ value decreases, unstable time-periodic solutions with more complex spatiotemporal structures appear, and determination of such solutions is supposed to be more challenging [6]. But we find that the Newton-CG method can handle such solutions with ease as well. To demonstrate, we now take $\gamma = 0.015$. Regarding the initial condition for Newton-CG iterations, the strategy of random trials has difficulty now due to the complex structure of the solution. Thus we switch to the “looking for approximate recurrence” strategy (the second strategy described in the last paragraph of section 2). Specifically, we simulate the evolution of the KS equation (41) from the initial condition $u(x, 0) = -\sin x$. We notice that the evolution solution in the time interval of $3.49 \leq t \leq 4.21$ is approximately time-periodic, thus we use this time-segment of the evolution solution as the initial condition for Newton-CG iterations.

This initial condition proves to converge to an exact time-periodic solution under Newton-CG iterations, and the numerical results are displayed in figure 2 (here we use 128 grid points rather than 64 points along each of the x and τ directions since the spatiotemporal structure of the present solution is more complex). The MATLAB code for this figure is the same as that in Appendix A, except for the γ value, the initial condition u_0 , the number of grid points in (x, τ) , and one of the plotting commands.

Panel (a) of figure 2 shows the difference $u_0(x, t) - u(x, t)$ between our initial condition $u_0(x, t)$ and the accurate time-periodic solution $u(x, t)$ (for two time periods). One can see that this difference is not small, meaning that our initial condition is not very close to the exact solution; but Newton-CG iterations still converge. The converged (accurate) solution is displayed in panel (b), and the accurate temporal period is found to be $T = 0.7294854797$. Notice that this time-periodic solution is more complex than the one in figure 1. Convergence rates of Newton-CG iterations are shown in panels (c, d), where the error versus the number of CG iterations and versus time are plotted respectively. One can see that this error drops from the original 280 to the final 10^{-9} in about 50,000 CG iterations, or 2.6 minutes.

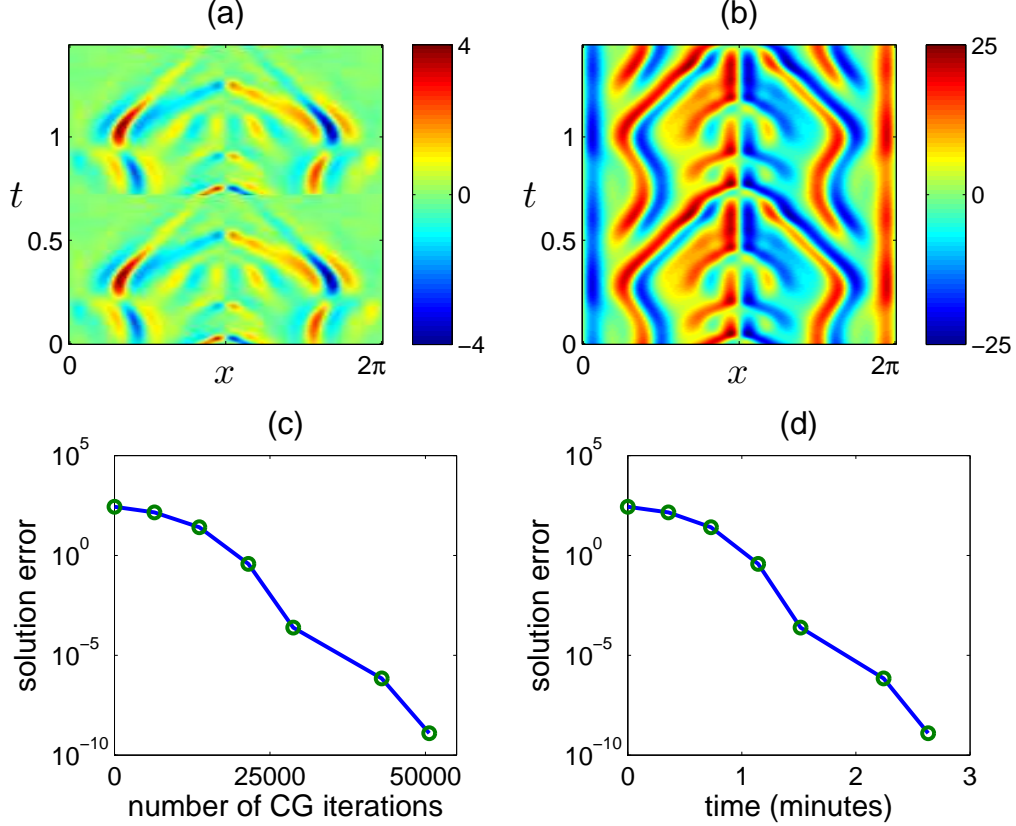


FIG. 2: Numerical computation of the time-periodic solution in the KS equation (41) at $\gamma = 0.015$. (a) Difference between the initial condition $u_0(x, t)$ and the accurate solution $u(x, t)$. (b) The accurate solution $u(x, t)$. (c) Error versus the number of CG iterations. (d) Error versus time. In (a, b), two time periods are shown. In (c, d), circles are Newton-iteration points.

Example 2 Our second example is the cubic-quintic Ginzburg-Landau (CQGL) equation (19), i.e.,

$$A_t = \chi A + \gamma A_{xx} - \beta |A|^2 A - \delta |A|^4 A, \quad (45)$$

where coefficients γ, β, δ are complex, and χ real (note that if χ is complex, its imaginary part can be eliminated by a trivial gauge transformation). This equation admits relative time-periodic solutions $A(x, t) = e^{i\mu t} U(x, t)$, where $U(x, t)$ is time-periodic and spatially localized [7, 22, 23]. Both the propagation constant μ and the temporal period

T in these solutions are unknown priori and need to be determined along with the solution $U(x, t)$. Below we use the numerical algorithm of section 3 to determine these relative time-periodic solutions.

The CQGL equation (45) is of the form (21), thus the numerical algorithm of section 3 directly applies. In this algorithm, the function G , as defined in (24), is

$$G = \chi U + \gamma U_{xx} - \beta |U|^2 U - \delta |U|^4 U.$$

Splitting the real and imaginary parts of the complex constants γ, β, δ and complex functions U, G as

$$\gamma = \gamma_1 + i\gamma_2, \quad \beta = \beta_1 + i\beta_2, \quad \delta = \delta_1 + i\delta_2, \quad U = u + iv, \quad G = g + ih,$$

we get

$$\begin{aligned} g &= \gamma_1 u_{xx} - \gamma_2 v_{xx} + \chi u - (\beta_1 u - \beta_2 v)(u^2 + v^2) - (\delta_1 u - \delta_2 v)(u^2 + v^2)^2, \\ h &= \gamma_1 v_{xx} + \gamma_2 u_{xx} + \chi v - (\beta_1 v + \beta_2 u)(u^2 + v^2) - (\delta_1 v + \delta_2 u)(u^2 + v^2)^2. \end{aligned}$$

The linearization operator \mathbf{G}_1 of functions $[g, h]^T$ is

$$\mathbf{G}_1 = \begin{bmatrix} \gamma_1 \partial_{xx} + G_{11} & -\gamma_2 \partial_{xx} + G_{12} \\ \gamma_2 \partial_{xx} + G_{21} & \gamma_1 \partial_{xx} + G_{22} \end{bmatrix}, \quad (46)$$

where

$$\begin{aligned} G_{11} &= \chi - \beta_1(u^2 + v^2) - 2u(\beta_1 u - \beta_2 v) - \delta_1(u^2 + v^2)^2 - 4u(\delta_1 u - \delta_2 v)(u^2 + v^2), \\ G_{12} &= \beta_2(u^2 + v^2) - 2v(\beta_1 u - \beta_2 v) + \delta_2(u^2 + v^2)^2 - 4v(\delta_1 u - \delta_2 v)(u^2 + v^2), \\ G_{21} &= -\beta_2(u^2 + v^2) - 2u(\beta_1 v + \beta_2 u) - \delta_2(u^2 + v^2)^2 - 4u(\delta_1 v + \delta_2 u)(u^2 + v^2), \\ G_{22} &= \chi - \beta_1(u^2 + v^2) - 2v(\beta_1 v + \beta_2 u) - \delta_1(u^2 + v^2)^2 - 4v(\delta_1 v + \delta_2 u)(u^2 + v^2). \end{aligned}$$

The adjoint operator of \mathbf{G}_1 is then $\mathbf{G}_1^A = \mathbf{G}_1^T$, i.e.,

$$\mathbf{G}_1^A = \begin{bmatrix} \gamma_1 \partial_{xx} + G_{11} & \gamma_2 \partial_{xx} + G_{21} \\ -\gamma_2 \partial_{xx} + G_{12} & \gamma_1 \partial_{xx} + G_{22} \end{bmatrix}. \quad (47)$$

Using the above formulae, the normal equation for Newton corrections $\Delta \mathbf{u}_n = [\Delta u_n, \Delta v_n]^T$ is

$$\mathbf{L}_{1n}^A \mathbf{L}_{1n} \Delta \mathbf{u}_n = -\mathbf{L}_{1n}^A \mathbf{L}_0(\mathbf{u}_n), \quad (48)$$

where \mathbf{L}_1 is given by equations (35), (36), (46), \mathbf{L}_1^A given by equations (39), (40), (47), and $\mathbf{L}_0(\mathbf{u})$ given by equation (32). This normal equation will be solved by preconditioned CG iterations.

Regarding the choice of the preconditioner \mathbf{M} , we follow the general guideline in the end of section 2. Specifically, by retaining only the highest (x, τ) -derivatives of Ψ in the normal-equation's linear operator $\mathbf{L}_1^A \mathbf{L}_1 \Psi$, we get

$$\mathbf{L}_1^A \mathbf{L}_1 \approx (|\gamma|^2 \partial_{xxxx} - \omega^2 \partial_{\tau\tau}) \mathbf{I}_2,$$

where \mathbf{I}_2 is a 2×2 identity matrix. Since the preconditioner must be positive-definite, we then choose the preconditioner as

$$\mathbf{M} = (c + |\gamma|^2 \partial_{xxxx} - \omega^2 \partial_{\tau\tau}) \mathbf{I}_2, \quad (49)$$

where c is a positive constant (which we set as $c = 8$). In execution, the ω value in this preconditioner will be obtained from the numerical solution \mathbf{u}_n through the quasi-Rayleigh quotient (31).

We now apply the above Newton-CG method to compute relative time-periodic solutions. First, we choose the parameter values in the CQGL equation (45) as

$$\gamma = 0.9 - 1.1i, \quad \beta = -3 - i, \quad \delta = 2.75 - i, \quad \chi = -0.1. \quad (50)$$

For this set of parameter values, the CQGL equation admits a stable relative-time-periodic and spatially-localized solution [22]. Since this solution is stable, we can use the time-evolution method (the second strategy in the end of section 2) to prepare our initial condition for Newton-CG iterations. Specifically, we numerically simulate the evolution of equation (45) from a Gaussian initial condition $A(x, 0) = e^{-x^2/10}$. This evolution gradually converges to a relative-time-periodic solution with temporal period of approximately 7.98 and propagation constant of approximately 2.04. Thus we take the time-segment $200 \leq t \leq 207.98$ of this solution $A(x, t)$, multiplied by the phase factor of $e^{-2.04it}$, as our initial condition $U(x, t)$ for Newton-CG iterations. The x -interval is taken as $-50 \leq x \leq 50$, discretized evenly by 512 grid points, and the τ direction is discretized evenly by 32 grid points. Since the solution is spatially localized and temporally periodic, we will use discrete Fourier transform to compute all derivatives. The MATLAB code for this computation is displayed in Appendix B. This code, together with the initial condition $U_0(x, t)$, is also posted at the author's homepage.

The numerical result from this MATLAB code is given in figure 3. This code converges to a time-periodic solution $U(x, t)$, whose amplitude and phase fields are shown in panels (a, b) (for two temporal periods). The accurate temporal period is found to be $T = 7.9820986731$, and the accurate propagation constant is $\mu = 2.0422917024$. Convergence speeds of these Newton-CG iterations are displayed in panels (c, d), where the error versus number of CG iterations and versus time are plotted. The error here is also defined as the maximum magnitude of the equation's residue, i.e., $\max|L_0(\mathbf{u}_n)|$. Panel (c) shows that this error drops from the initial value of about 0.3 to the final value below 10^{-10} under 2800 CG iterations, while panel (d) shows that this drop of the error takes about 1.3 minutes.

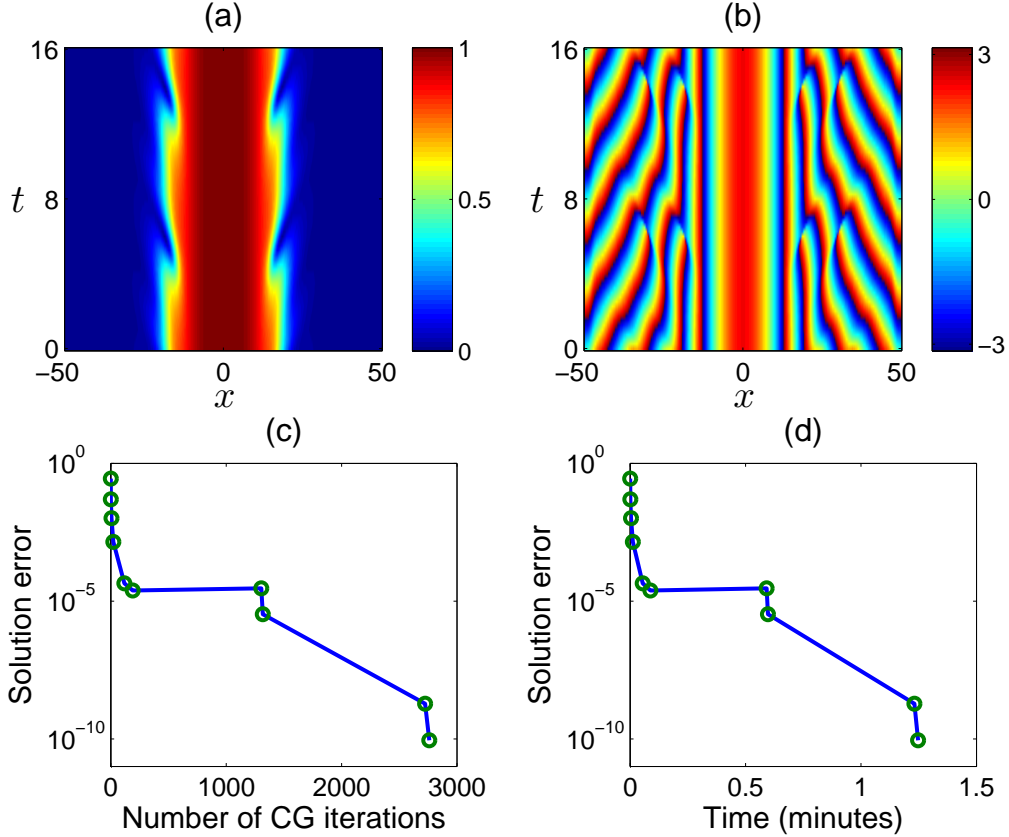


FIG. 3: Numerical computation of the relative time-periodic solution in the cubic-quintic Ginzburg-Landau equation (45) with parameter values (50). (a, b) Amplitude and phase of solution $U(x, t)$. (c) Error versus the number of CG iterations. (d) Error versus time. In (a, b), two time periods are shown. In (c, d), circles are Newton-iteration points. This figure is produced by the MATLAB code in Appendix B.

When parameters in the CQGL equation (45) change, this stable relative-time-periodic solution in figure 3 can

lose its stability. For instance, when $\text{Re}(\gamma)$ decreases below 0.88 and the other parameters fixed, this solution would become unstable [22]. Such unstable solutions can be computed accurately by our Newton-CG method as well. Indeed, starting from the stable solution of figure 3 and using the continuation method (the third strategy in the end of section 2), we can track the entire branch of this solution family parameterized by $\text{Re}(\gamma)$, and the results are shown in figure 4. Here dependences of the propagation constant μ and temporal period T on $\text{Re}(\gamma)$ are displayed in panels (a, b), and the accurate unstable solution at $\text{Re}(\gamma)=0.85$ (with error less than 10^{-10}) is plotted in panel (c). As can be seen, this continuation by Newton-CG methods is very suitable for studying bifurcations of time-periodic solutions.

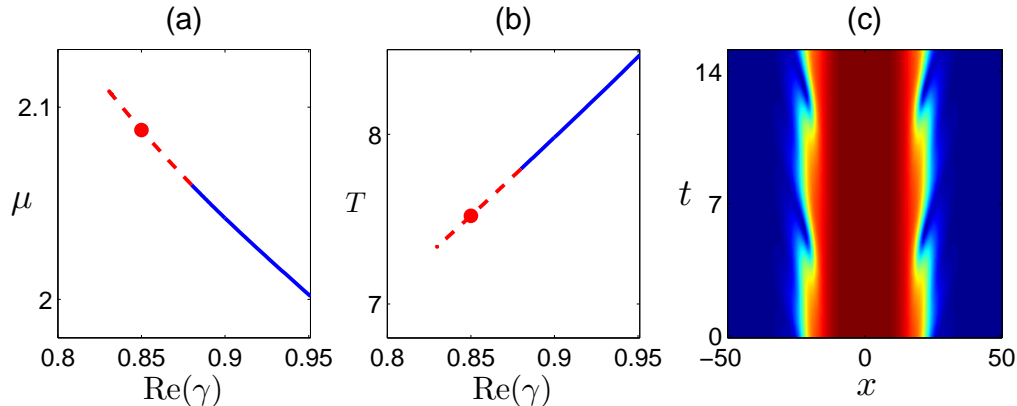


FIG. 4: Continuation of Newton-CG methods for tracing the entire family of a relative time-periodic solution in the CQGL equation (45), starting from the stable solution in figure 3 (at $\text{Re}(\gamma)=0.9$). Here parameters are as given in equation (50), except that $\text{Re}(\gamma)$ is allowed to vary. (a, b) Graphs of the propagation constant μ and temporal period T versus $\text{Re}(\gamma)$; (c) Amplitude field of the solution $U(x,t)$ at $\text{Re}(\gamma)=0.85$ [marked by a red dot in (a, b)].

Our numerical algorithms for time-periodic solutions were intended for dissipative wave equations, such as the KS equation (41) and the CQGL equation (45). But they certainly apply to systems of ODEs as well. For systems of ODEs, a number of numerical methods have already been developed to compute their periodic orbits (see [6, 9–13] for instance). Here we apply our numerical methods to systems of ODEs and demonstrate their easy computation of periodic orbits in such systems.

Example 3 The example of systems of ODEs we consider is the familiar Lorenz equations [26]

$$\frac{dx}{dt} = \sigma(y - x), \quad (51)$$

$$\frac{dy}{dt} = rx - y - xz, \quad (52)$$

$$\frac{dz}{dt} = xy - bz, \quad (53)$$

where (x, y, z) are real variables of time, and σ, r, b are real constants. These equations admit many types of periodic orbits in wide ranges of parameter values (see [27] and the references therein). Below we formulate our numerical algorithm to compute these periodic orbits.

Periodic orbits in Lorenz equations contain a single unknown parameter, which is their period. Thus the algorithm of section 2 applies. In this case, the function \mathbf{F} in the algorithm of section 2 is

$$\mathbf{F}(\mathbf{u}) = \begin{pmatrix} \sigma(y - x) \\ rx - y - xz \\ xy - bz \end{pmatrix},$$

where $\mathbf{u} = [x, y, z]^T$. The linearization operator of this function (i.e., the Jacobian) is

$$\mathbf{F}_1 = \begin{pmatrix} -\sigma & \sigma & 0 \\ r - z & -1 & -x \\ y & x & -b \end{pmatrix},$$

and its adjoint operator is $\mathbf{F}_1^A = \mathbf{F}_1^T$. The quasi-normal Newton-correction equation (18) for the Lorenz equations then is

$$\mathbf{P}_n^A \mathbf{L}_{1n} \Delta u_n = -\mathbf{P}_n^A \mathbf{L}_0(u_n), \quad (54)$$

where

$$\mathbf{L}_0(\mathbf{u}) = \omega \mathbf{u}_\tau - \mathbf{F}, \quad \mathbf{L}_1 \Psi \equiv \mathbf{P} \Psi - \frac{\langle \mathbf{u}_\tau, \mathbf{P} \Psi \rangle}{\langle \mathbf{u}_\tau, \mathbf{u}_\tau \rangle} \mathbf{u}_\tau, \quad \mathbf{P} = \omega \partial_\tau - \mathbf{F}_1, \quad \mathbf{P}^A = -\omega \partial_\tau - \mathbf{F}_1^A, \quad \omega = \frac{\langle \mathbf{u}_\tau, \mathbf{F} \rangle}{\langle \mathbf{u}_\tau, \mathbf{u}_\tau \rangle},$$

and we solve it using preconditioned CG iterations.

Regarding the preconditioner, by retaining only the derivative terms of Ψ in $\mathbf{P}^A \mathbf{L}_1 \Psi$, we get $\mathbf{P}^A \mathbf{L}_1 \approx -\omega^2 \partial_{\tau\tau} \mathbf{I}_3$, where \mathbf{I}_3 is the 3×3 identity matrix. Thus we choose the preconditioner as

$$\mathbf{M} = (c - \omega^2 \partial_{\tau\tau}) \mathbf{I}_3, \quad (55)$$

where c is a positive number (which we take as $c = 30$).

Now we apply the above Newton-CG method to compute periodic orbits in the Lorenz equations. As an example, we take $\sigma = 10$ and $b = \frac{8}{3}$, the same values Lorenz used in his pioneering paper [26]. At these σ and b values, a subcritical Hopf bifurcation occurs at $r = r_H \approx 24.74$, where the pair of fixed points $(x_c, y_c, z_c) = (\pm\sqrt{b(r-1)}, \pm\sqrt{b(r-1)}, r-1)$ lose their stability when $r > r_H$. When $r < r_H$, an unstable limit cycle appears [27]. This behavior is illustrated in figure 5 [panel (a)].

We now compute this unstable limit cycle below r_H , with $r = 24$ for definiteness. The initial condition for Newton-CG iterations is chosen by random trials, which yield many successful choices, one of which being

$$x_0(\tau) = x_c - 2.5 \cos(\tau + 0.5), \quad y_0(\tau) = y_c + 3 \sin(\tau - 0.4); \quad z_0(\tau) = z_c - 4 \cos(\tau - 0.3). \quad (56)$$

We also discretize time evenly by 256 points. The MATLAB code for this computation is provided in Appendix C.

The numerical outcome of this MATLAB code is given in figure 5 [panels (b,c,d)]. In panel (b), the accurate limit cycle is displayed. The accurate period is found to be $T = 0.6793367642$. Convergence speeds of Newton-CG iterations are shown in panels (c, d). We see that the error (defined by $\max|\mathbf{L}_0(\mathbf{u}_n)|$ as before) drops from the initial value of about 12 to the final value below 10^{-11} in 150 CG iterations, or under 0.04 seconds.

When $r = 28$ (above the Hopf bifurcation point r_H), a strange attractor appears [26]. On this strange attractor, an infinite number of unstable periodic orbits exist. To look for these periodic orbits, we apply the above numerical algorithm, starting from initial conditions

$$\begin{aligned} x_0(\tau) &= x_c + \sum_{k=1}^2 [A_{1k} \cos(k\tau) + B_{1k} \sin(k\tau)], \\ y_0(\tau) &= y_c + \sum_{k=1}^2 [A_{2k} \cos(k\tau) + B_{2k} \sin(k\tau)], \\ z_0(\tau) &= z_c + \sum_{k=1}^2 [A_{3k} \cos(k\tau) + B_{3k} \sin(k\tau)], \end{aligned}$$

where coefficients A_{ij} and B_{ij} are taken randomly from the interval $[-10, 10]$. Repeatedly running the MATLAB code of Appendix C, with r changed to 28, the initial condition changed to the above random functions, and `errorCG` changed to 10^{-2} , we found 20 distinct periodic orbits with period below 10 and accuracy 10^{-10} in 5 minutes.

V. SUMMARY

A numerical method was proposed for computing time-periodic and relative time-periodic solutions in general dissipative wave systems. Since the temporal period and possibly other additional internal parameters in the solution are unknown priori, our idea was to first express those unknown parameters in terms of the solution through quasi-Rayleigh quotients, so that the resulting integro-differential equation is for the time-periodic solution only. Then this

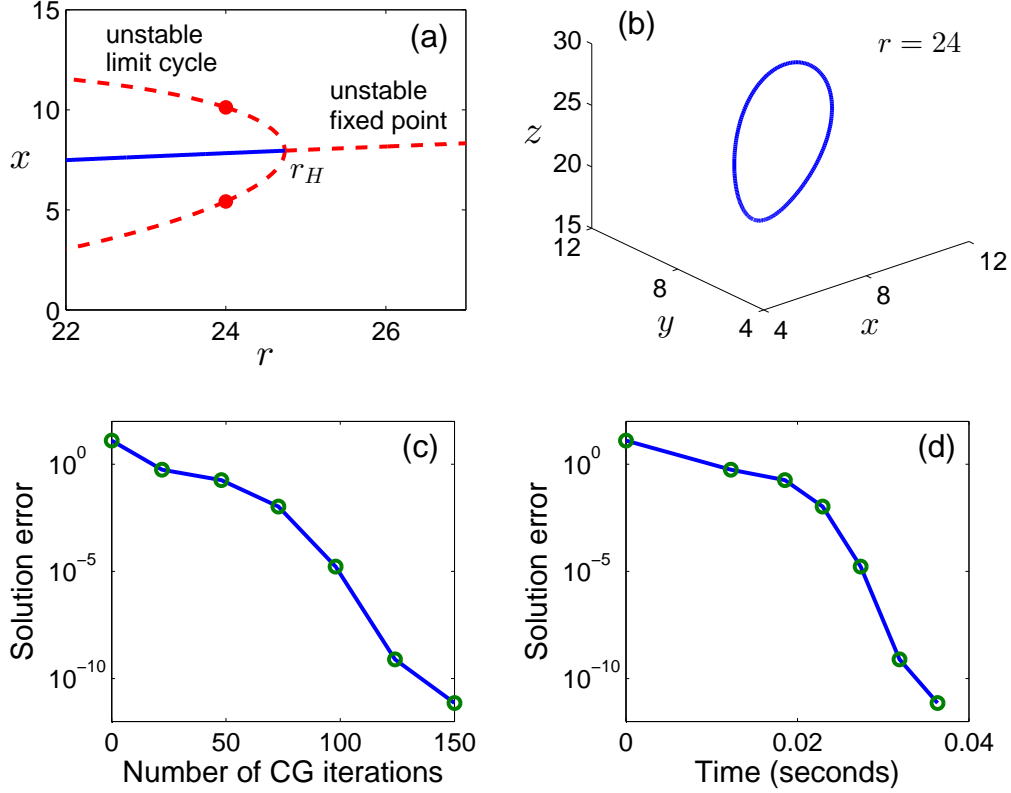


FIG. 5: Numerical computation of an unstable limit cycle in the Lorenz equations for parameter values of $\sigma = 10$, $b = \frac{8}{3}$, and $r = 24$. (a) Bifurcation diagram near the subcritical Hopf bifurcation point $r = r_H \approx 24.74$. (b) Numerically obtained limit cycle. (c) Error versus number of CG iterations. (d) Error versus time. This figure (b-d) is produced by the MATLAB code in Appendix C.

integro-differential equation is computed in the combined spatiotemporal domain by Newton-conjugate-gradient iterations, where the Newton-correction equation is solved by preconditioned conjugate gradient iterations. Linearization operators and their adjoints in the Newton-correction equation were derived analytically for general systems, so that conjugate gradient iterations for Newton corrections can be readily implemented.

As numerical examples, we applied this method to the Kuramoto-Sivashinsky equation and the cubic-quintic Ginzburg-Landau equation, whose time-periodic or relative time-periodic solutions with spatially-periodic or spatially-localized profiles were computed. We also used this method to compute periodic orbits in the Lorenz equations, since this method applies to systems of ordinary differential equations as a special case.

Numerical examples showed that first, both stable and unstable time-periodic solutions can be obtained by this method. Second, the numerical accuracy of this method is spectral, since we used spectral differentiation (the discrete Fourier transform) to compute spatial and temporal derivatives. Thirdly, this method only took from a fraction of a second to a couple of minutes (on a personal computer) to find solutions of varying spatiotemporal complexities to the accuracy of 10^{-10} , thus this method is fast-converging and time-efficient. Fourthly, the coding of this method is short and simple. To make it evident, stand-alone MATLAB codes for our numerical examples are provided in the appendices.

This proposed method can be a powerful tool for numerically studying time-periodic (and relative time-periodic) solutions and their bifurcations in physical systems.

Acknowledgment

This work was supported in part by the Air Force Office of Scientific Research (grant USAF 9550-12-1-0244) and the National Science Foundation (grant DMS-1311730).

Appendix A: MATLAB code for the Kuramoto-Sivashinsky equation

In this appendix, we provide the MATLAB code for computing an unstable time- and space-periodic solution in the Kuramoto-Sivashinsky equation (41) with $\gamma = 0.054$. The output of this code is shown in figure 1.

```
% Newton-CG method for computing time-space-periodic solutions
% in the KS equation:  $u_t + uu_x + u_{xx} + \gamma u_{xxxx} = 0$ .
% In this code, z represents scaled time tau in the paper.

gamma=0.054; Nx=64; Nz=64; Lx=2*pi; Lz=2*pi; errormax=1e-9; errorCG=1e-4;
dx=Lx/Nx; x=0:dx:Lx-dx; kx=[0:Nx/2-1 -Nx/2:-1]*2*pi/Lx;
dz=Lz/Nz; z=0:dz:Lz-dz; kz=[0:Nz/2-1 -Nz/2:-1]*2*pi/Lz;
[X,Z]=meshgrid(x,z); [KX,KZ]=meshgrid(kx,kz); KX2=-KX.*KX+gamma*KX.^4;
u0=-7*sin(3*X)-3*sin(Z).*(sin(4*X)-sin(5*X))-cos(Z).*sin(X); u=u0; % i.c.

tic; nnt=0; ncg=0; % nnt: # of Newton steps; ncg: # of CG iterations
while 1 % Newton-CG iterations for periodic solutions start
    nnt=nnt+1;
    ufft=fft2(u);
    F=-real(u.*ifft2(i*KX.*ufft)+ifft2(KX2.*ufft));
    uz=real(ifft2(i*KZ.*ufft));
    omega=sum(sum(uz.*F))/sum(sum(uz.*uz));
    LOu=omega*uz-F;
    uerror(nnt)=max(max(abs(LOu))); uerror(nnt)
    numcg(nnt)=ncg; time(nnt)= toc;
    if uerror(nnt) < errormax
        break
    end

P=@(W) real(ifft2((omega*i*KZ+KX2).*fft2(W))+ifft2(i*KX.*fft2(u.*W)));
PA=@(W) real(ifft2((-omega*i*KZ+KX2).*fft2(W))-u.*ifft2(i*KX.*fft2(W)));

c=30; fftM=omega^2*KZ.*KZ+KX2.*KX2+c; % Preconditioner
du=0*Z; % CG iterations start
R=-PA(LOu);
MinvR=real(ifft2(fft2(R)./fftM));
R2=sum(sum(R.*MinvR)); R20=R2;
D=MinvR;
while (R2 > R20*errorCG^2)
    PD=P(D);
    L1D=PD-sum(sum(uz.*PD))/sum(sum(uz.*uz))*uz;
    PAL1D=PA(L1D);
    a=R2/sum(sum(D.*PAL1D));
    du=du+a*D;
    R=R-a*PAL1D;
    MinvR=real(ifft2(fft2(R)./fftM));
    R2old=R2;
```

```

R2=sum(sum(R.*MinvR));
b=R2/R2old;
D=MinvR+b*D;
ncg=ncg+1;
end % CG iterations end
u=u+du;
end % Newton-CG iterations end

% plotting of numerical results
subplot(221); imagesc(x, [z z+Lz], [u0; u0]); axis xy; colorbar;
xlabel('x'); ylabel('\tau', 'rotation', 0); title('(a)');
subplot(222); imagesc(x, [z z+Lz]/omega, [u; u]); axis xy; colorbar;
xlabel('x'); ylabel('t', 'rotation', 0); title('(b)');
subplot(223); semilogy(numcg, uerror, numcg, uerror, 'o');
xlabel('number of CG iterations'); ylabel('solution error'); title('(c)');
subplot(224); semilogy(time, uerror, time, uerror, 'o');
xlabel('time (seconds)'); ylabel('solution error'); title('(d)');
format long; period=2*pi/omega

```

Appendix B: MATLAB code for the cubic-quintic Ginzburg-Landau equation

In this appendix, we provide the MATLAB code for computing a (stable) relative-time-periodic and space-localized solution in the cubic-quintic Ginzburg-Landau equation (45) with parameters (50). The initial condition `U0_fig3.mat` in this code is obtained from simulating the CQGL equation from a Gaussian initial condition $A(x, 0) = e^{-x^2/10}$ (see text for details). The MATLAB data for this initial condition can be found at the author's homepage www.cems.uvm.edu/~jxyang/codes.htm. From this initial approximation (whose error is about 0.3), the following MATLAB code then drives the error below 10^{-10} , and the output of this code is shown in figure 3. Note that during MATLAB implementation of the algorithm, real functions u and v are recombined into $U = u + iv$, so that they can be computed simultaneously for numerical efficiency and compact coding. Because of it, real operators \mathbf{P} , \mathbf{P}^A , L_1 and L_1^A in the algorithm are adjusted into complex operators, and some inner products are expressed through these complex functions.

```

% Newton-CG method for computing time-periodic and space-localized solutions
% in the CQGL equation: At-gamma*Axx+beta*|A|^2A+delta*|A|^4A-chi*A=0.
% In this code, z represents scaled time tau, and A=U*exp(i*mu*t).

load U0_fig3.mat; % this data contains initial condition U(x, z)
Lx=100; Nx=512; Lz=2*pi; Nz=32; errormax=1e-10; errorCG=1e-4;
dx=Lx/Nx; x=-Lx/2:dx:Lx/2-dx; kx=[0:Nx/2-1 -Nx/2:-1]*2*pi/Lx;
dz=Lz/Nz; z=0:dz:Lz-dz; kz=[0:Nz/2-1 -Nz/2:-1]*2*pi/Lz;
[X,Z]=meshgrid(x,z); [KX,KZ]=meshgrid(kx,kz); KX2=KX.*KX;

gamma=0.9-1.1i; beta=-3-i; delta=2.75-i; chi=-0.1;
gamma1=real(gamma); gamma2=imag(gamma); beta1=real(beta); beta2=imag(beta);
delta1=real(delta); delta2=imag(delta);

tic; nnt=0; ncg=0; % nnt: # of Newton steps; ncg: # of CG iterations
while 1 % Newton-CG iterations for periodic solutions start
    nnt=nnt+1;
    u=real(U); v=imag(U); U2=u.*u+v.*v; U4=U2.*U2;
    G=gamma*ifft2(-KX2.*fft2(U))-(beta*U2+delta*U4-chi).*U;
    Ut=ifft2(i*KZ.*fft2(U)); ut=real(Ut); vt=imag(Ut);

```

```

produv=2*sum(sum(u.*v)); produitvt=2*sum(sum(ut.*vt));
mu = sum(sum(v.*imag(G)-u.*real(G)))/produv;
omega= sum(sum(ut.*imag(G)+vt.*real(G)))/produitvt;
LOU=omega*Ut+i*mu*U-G;
Uerror(nnt)=max(max(abs(LOU))); Uerror(nnt)
numcg(nnt)=ncg; time(nnt)= toc;
if Uerror(nnt) < errormax
    break
end

betaU1=beta1*u-beta2*v;    betaU2=beta1*v+beta2*u;
deltaU1=delta1*u-delta2*v; deltaU2=delta1*v+delta2*u;
G11=chi-beta1*U2-betaU1*2.*u-delta1*U4-deltaU1*4.*u.*U2;
G12= +beta2*U2-betaU1*2.*v+delta2*U4-deltaU1*4.*v.*U2;
G21= -beta2*U2-betaU2*2.*u-delta2*U4-deltaU2*4.*u.*U2;
G22=chi-beta1*U2-betaU2*2.*v-delta1*U4-deltaU2*4.*v.*U2;
Dxx=@(F)  ifft2(-KX2.*fft2(F));
Dtxx=@(F)  ifft2(( omega*i*KZ+gamma1*KX2).*fft2(F));
DtxxA=@(F)  ifft2((-omega*i*KZ+gamma1*KX2).*fft2(F));

P=@(F)  Dtxx(real(F))-G11.*real(F)-(mu+G12).*imag(F)+gamma2*Dxx(imag(F)) ...
+i*( (mu-G21).*real(F)-gamma2*Dxx(real(F))+Dtxx(imag(F))-G22.*imag(F) );
PA=@(F)  DtxxA(real(F))-G11.*real(F)+(mu-G21).*imag(F)-gamma2*Dxx(imag(F)) ...
+i*( -(mu+G12).*real(F)+gamma2*Dxx(real(F))+DtxxA(imag(F))-G22.*imag(F) );

L1= @(F) P(F)-sum(sum(imag(Ut.*P(F))))/produitvt*Ut ...
+sum(sum(real(U.*P(F))))/produv*i*U;
L1A=@(F) PA(F)-sum(sum(real(conj(F).*Ut)))/produitvt*PA(vt+i*ut) ...
-sum(sum(imag(conj(F).*U)))/produv*PA(u-i*v);

c=8; fftM=omega^2*KZ.*KZ+abs(gamma)^2*KX2.*KX2+c;    % Preconditioner
dU=0*Z;    % CG iterations start
R=-L1A(LOU);
MinvR=ifft2(fft2(R)./fftM);
R2=sum(sum(real(conj(R).*MinvR))); R20=R2;
D=MinvR;
while (R2 > R20*errorCG^2)
    L2D=L1A(L1(D));
    a=R2/sum(sum(real(conj(D).*L2D)));
    dU=dU+a*D;
    R=R-a*L2D;
    MinvR=ifft2(fft2(R)./fftM);
    R2old=R2;
    R2=sum(sum(real(conj(R).*MinvR)));
    b=R2/R2old;
    D=MinvR+b*D;
    ncg=ncg+1;
end
U=U+dU;
end

% plotting of numerical results
subplot(221); imagesc(x, [z z+Lz]/omega, abs([U;U])); axis xy; colorbar;
xlabel('x'); ylabel('t'); title('(a)');

```

```

subplot(222); imagesc(x, [z z+Lz]/omega, angle([U;U])); axis xy; colorbar;
xlabel('x'); ylabel('t'); title('(b)');
subplot(223); semilogy(numcg, Uerror, numcg, Uerror, 'o');
xlabel('number of CG iterations'); ylabel('solution error'); title('(c)');
subplot(224); semilogy(time/60, Uerror, time/60, Uerror, 'o');
xlabel('time (minutes)'); ylabel('solution error'); title('(d)');
format long; period=2*pi/omega
mu

```

Appendix C: MATLAB code for the Lorenz equation

In this appendix, we provide the MATLAB code for computing an unstable limit cycle in the Lorenz equations with $\sigma = 10$, $b = 8/3$ and $r = 24$. This limit cycle is located below the subcritical Hopf bifurcation point $r_H \approx 24.74$. The output of this code is shown in figure 5(b-d).

```

% Newton-CG method for computing limit cycles in the Lorenz equations.

L=2*pi; N=256; errormax=1e-10; errorCG=1e-4;
dtau=L/N; tau=(0:dtau:L-dtau)';
ktau=[0:N/2-1 -N/2:-1]*2*pi/L; Ktau=[ktau ktau ktau];

sigma=10; b=8/3; r=24; xc=sqrt(b*(r-1)); yc=xc; zc=r-1;
x=xc-2.5*cos(tau+0.5); y=yc+3*sin(tau-0.4); z=zc-4*cos(tau-0.3); u=[x y z];

tic; nnt=0; ncg=0; % nnt: # of Newton steps; ncg: # of CG iterations
while 1 % Newton-CG iterations for limit cycles start
    nnt=nnt+1;
    F=[sigma*(y-x) r*x-y-x.*z x.*y-b*z];
    utau=real(ifft(i*Ktau.*fft(u)));
    omega=sum(sum(utau.*F))/sum(sum(utau.*utau));
    LOu=omega*utau-F;
    uerror(nnt)=max(max(abs(LOu))); uerror(nnt)
    numcg(nnt)=ncg; time(nnt)= toc;
    if uerror(nnt) < errormax
        break
    end

    P=@(W) omega*real(ifft(i*Ktau.*fft(W))) ...
        -[-sigma*W(:,1)+sigma*W(:,2), ...
          (r-z).*W(:,1)-W(:,2)-x.*W(:,3), ...
          y.*W(:,1)+x.*W(:,2)-b*W(:,3)];

    PA=@(W) -omega*real(ifft(i*Ktau.*fft(W))) ...
        -[-sigma*W(:,1)+(r-z).*W(:,2)+y.*W(:,3), ...
          sigma*W(:,1)-W(:,2)+x.*W(:,3), ...
          -x.*W(:,2)-b*W(:,3)];

    c=30; fftM=omega^2*Ktau.*Ktau+c; % Preconditioner
    du=0*u; % CG iterations start
    R=-PA(LOu);
    MinvR=real(ifft(fft(R)./fftM));
    R2=sum(sum(R.*MinvR)); R20=R2;

```

```

D=MinvR;
while (R2 > R20*errorCG^2)
    PD=P(D);
    L1D=PD-sum(sum(utau.*PD))/sum(sum(utau.*utau))*utau;
    PAL1D=PA(L1D);
    a=R2/sum(sum(D.*PAL1D));
    du=du+a*D;
    R=R-a*PAL1D;
    MinvR=real(iff(fft(R)./fftM));
    R2old=R2;
    R2=sum(sum(R.*MinvR));
    beta=R2/R2old;
    D=MinvR+beta*D;
    ncg=ncg+1;
end
                                % CG iterations end
u=u+du;
x=u(:,1); y=u(:,2); z=u(:,3);
end
                                % Newton-CG iterations end

% plotting of numerical results
subplot(222); plot3(x, y, z); xlabel('x'); ylabel('y'); zlabel('z');
title('b'); axis([4 12 4 12 15 30]); view([-40 30])
subplot(223); semilogy(numcg, uerror, numcg, uerror, 'o');
xlabel('number of CG iterations'); ylabel('solution error'); title('c');
subplot(224); semilogy(time, uerror, time, uerror, 'o');
xlabel('time (seconds)'); ylabel('solution error'); title('d');
format long; period=2*pi/omega

```

-
- [1] J.M. Soto-Crespo, N. Akhmediev and G. Town, “Interrelation between various branches of stable solitons in dissipative systems – conjecture for stability criterion”, *Opt. Comm.* 199, 283–293 (2001).
- [2] J. Yang, *Nonlinear Waves in Integrable and Nonintegrable Systems* (SIAM, Philadelphia, 2010).
- [3] J. Yang and T.I. Lakoba, “Universally-convergent squared-operator iteration methods for solitary waves in general nonlinear wave equations”, *Stud. Appl. Math.* 118, 153–197 (2007).
- [4] R. Artuso, E. Aurell, and P. Cvitanović, “Recycling of strange sets: I. Cycle expansions”, *Nonlinearity* 3, 325–359 (1990).
- [5] S.M. Zoldi and H.S. Greenside, “Spatially localized unstable periodic orbits of a high-dimensional chaotic system”, *Phys. Rev. E* 57, R2511–2514 (1998).
- [6] Y. Lan and P. Cvitanovic, “Variational method for finding periodic orbits in a general flow”, *Phys. Rev. E* 69, 016217 (2004).
- [7] V. Lopez, P. Boyland, M.T. Heath and R.D. Moser, “Relative periodic solutions of the complex GinzburgLandau equation”, *SIAM J. Appl. Dyn. Sys.* 4, 1042–1075 (2005).
- [8] I.V. Barashenkov, E.V. Zemlyanaya and T. C. van Heerden, “Time-periodic solitons in a damped-driven nonlinear Schrödinger equation”, *Phys. Rev. E* 83, 056609 (2011).
- [9] D. Morrison, J. Riley, and J. Zancanaro, “Multiple shooting method for two-point boundary value problems,” *Comm. ACM*, 5, 613–614 (1962).
- [10] U. Ascher, J. Christiansen and R. D. Russell, “A collocation solver for mixed order systems of boundary value problems”, *Math. Comp.* 33, 659–679 (1979).
- [11] F. H. Ling and X. X. Wu, “Fast Galerkin method and its application to determine periodic solutions of non-linear oscillators”, *Internat. J. Non-Linear Mech.* 22, 8998 (1987).
- [12] J. Guckenheimer and B. Meloon, “Computing periodic orbits and their bifurcations with automatic differentiation”, *SIAM J. Sci. Comput.* 22, 951–985 (2000).
- [13] E.J. Doedel, H.B. Keller and J.P. Kernévez, “Numerical analysis and control of bifurcation problems (II): Bifurcation in infinite dimensions”, *Int. J. Bifurcation and Chaos* 1, 745–772 (1991).
- [14] G. Golub and C. Van Loan, *Matrix Computations*, third ed. (The Johns Hopkins University Press, Baltimore, 1996).

- [15] J. Yang, “Newton-conjugate gradient methods for solitary wave computations”, *J. Comp. Phys.* 228, 7007–7024 (2009).
- [16] L.N. Trefethen, *Spectral method in matlab* (SIAM, Philadelphia, 2000).
- [17] J.P. Boyd, *Chebyshev and Fourier Spectral Methods* (2nd edition) (Dover, Mineola, NY, 2001).
- [18] Y. Kuramoto and T. Tsuzuki, “Persistent propagation of concentration waves in dissipative media far from thermal equilibrium”, *Progr. Theoret. Phys.* 55, 356-369 (1976).
- [19] G. Sivashinsky, “Nonlinear analysis of hydrodynamic instability in laminar flames I. Derivation of basic equations”, *Acta Astron.* 4, 1177–1206 (1977).
- [20] I.M. Hyman and B. Nicolaenko, “The Kuramoto-Sivashinsky equations, a bridge between PDEs and dynamical systems”, *Physica D*, 23, 113–126 (1986).
- [21] I.G. Kevrekidis, B. Nicolaenko and C. Scovel, “Back in the saddle again: A computer assisted study of Kuramoto-Sivashinsky equation”, *SIAM J. Appl. Math.* 50, 760–790 (1990).
- [22] R.J. Deissler and H.R. Brand, “Periodic, quasiperiodic, and chaotic localized solutions of the quintic complex Ginzburg-Landau equation”, *Phys. Rev. Lett.* 72, 478–481 (1994).
- [23] J. M. Soto-Crespo, N. Akhmediev, and A. Ankiewicz, “Pulsating, creeping, and erupting solitons in dissipative systems”, *Phys. Rev. Lett.* 85, 2937–2940 (2000).
- [24] R. LaQuey, S. Mahajan, P. Rutherford and W. Tang, “Nonlinear saturation of the trapped-ion mode”, *Phys. Rev. Lett.* 34, 391–394 (1975).
- [25] D.T. Papageorgiou and Y.S. Smyrlis, “The route to chaos for the Kuramoto-Sivashinsky equation”, *Theor. Comp. Fluid Dyn.* 3, 15–42 (1991).
- [26] E.N. Lorenz, “Deterministic nonperiodic flow”, *J. Atmos. Sci.* 20, 130–141 (1963).
- [27] S.H. Strogatz, *Nonlinear Dynamics and Chaos* (Perseus Books, Reading, Massachusetts, 1994).